Journal of Experimental and Theoretical Physics, Vol. 98, No. 3, 2004, pp. 556–564.
Translated from Zhurnal Éksperimental'noĭ i Teoreticheskoĭ Fiziki, Vol. 125, No. 3, 2004, pp. 630–639.

SOLIDS
Electronic Properties

The Band Structure of *n*-Type Cuprate Superconductors with the *T*'(*T*) Structure Taking into Account Strong Electron Correlation

V. A. Gavrichkov and S. G. Ovchinnikov

Kirenskiĭ Institute of Physics, Siberian Division, Russian Academy of Sciences, Akademgorodok, Krasnoyarsk, 660036 Russia

e-mail: gav@iph.Krasn.ru; sgo@iph.Krasn.ru

Received June 6, 2003

Abstract—The spectral density, dispersion relations, and the position of the Fermi level for *n*-doped compositions based on NCO and LCO were calculated within the framework of the generalized tight binding method. As distinguished from LCO, the dielectric gap in NCO is nonlinear in character. We observe a virtual level both at the bottom of the conduction band and at the top of the valence band in both compounds. However, its position corresponds to the extreme bottom of the conduction band in LCO and is 0.1–0.2 eV above the bottom in NCO. This explains why we observe Fermi level pinning in *n*-LCO as the concentration of the doping component grows and reproduce its absence in NCCO at low doping values. We also found both compositions to be unstable in a narrow concentration range with respect to a nonuniform charge density distribution. The relation between the phase diagram for NCCO and the calculated electronic structure is discussed. © *2004 MAIK "Nauka/Interperiodica".*

1. INTRODUCTION

Superconducting *n*-type cuprates $Nd_{2-x}Ce_xCuO_4$ (NCCO) and $Pr_{2-x}Ce_xCuO_4$ (PCCO) have certain special features that distinguish them from *p*-type cuprates. Rare-earth metal and oxygen layers are shifted in their crystal structure with respect to CuO_2 in such a way that there is no nearest neighbor (the apical oxygen) for copper along the *c* axis; that is, the structural element of the CuO_2 layer is a plane CuO_4 cluster, whereas it is a CuO_6 octahedron in $La_{2-x}Sr_xCuO_4$ (LSCO). The phase diagram of NCCO is substantially different from the phase diagram of LSCO (Fig. 1). The initial undoped Nd_2CuO_4 (NCO) composition is an antiferromagnet and dielectric. Doping with electrons rather weakly suppresses the antiferromagnetic state [1] because of the diamagnetic dilution mechanism [2]. The superconducting state borders on the antiferromagnetic phase and exists in a narrow concentration range $x_{min} < x < x_{max}$, where $x_{min} = 0.14$ and $x_{max} = 0.17$. In the normal state, the electrical conduction of NCCO is described by a Fermi-liquid quadratic temperature dependence [3], as distinguished from linear dependences for hole high-T_C superconductors [4]. It was shown for NCCO by angle-resolved photoelectron spectroscopy [5] that the dielectric gap in this compound was not rectilinear. The minimum of the conduction band and the maximum of the valence band belong to different Brillouin zone points, $\mathbf{k} = (\pi, 0)$ and $\mathbf{k} = (\pi/2, \pi/2)$, respectively. The dispersion relations in NCCO for the top of the valence band, however, remain virtually identical to those in LSCO. Angle-resolved photoelectron spectra also revealed the appearance of intragap states when either NCCO was doped with electrons or LSCO was doped with holes [5]. As distinguished from LSCO, where chemical potential pinning occurs at low *x*, NCCO shows a more complex concentration dependence of the chemical potential [6].

This is one more important difference between NCCO and LSCO, which is related to the possible role that neodymium *f* electrons can play in the formation of the state of heavy fermions at low temperatures [7]. However, first, no unambiguous experimental substan-

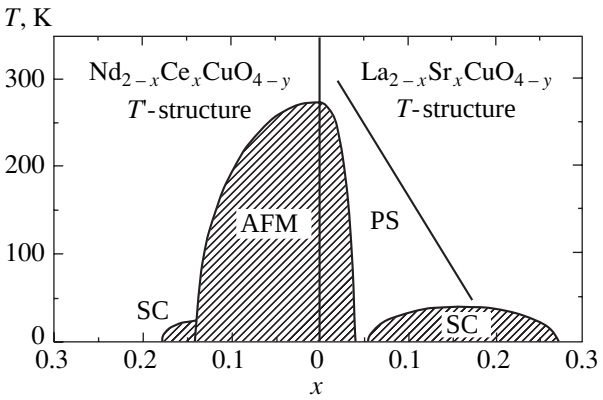

Fig. 1. Phase diagram of LSCO and NCCO. Composition regions: SC, superconducting phase; PS, pseudogap state; and AFM, dielectric phase in the antiferromagnetic state.

tiation [8] of the existence of such a state has been obtained and no explanation of the large coefficient γ value in the linear temperature dependence of heat capacity, $c = \gamma T$, where $\gamma \approx 4J/k^2$ for $x > 0.15$ [9], has been suggested. Secondly, at a low doping level ($0.05 \le x < 0.14$), the γ value is an order of magnitude smaller, $\gamma = 0.3J/k^2$ [9], which leads us to conclude that, even if the state of heavy fermions of the new type does exist in NCCO, these effects manifest themselves at higher concentrations because of the low Nd–Cu spin–spin coupling constant. In this work, we consider low doping levels, and, at $x < 0.15$, the beautiful physics of heavy fermions [7] remains outside the scope of our analysis.

The purpose of this work was to study the electronic structure of NCO and La_2CuO_4 (LCO) undoped and weakly doped with electrons. We use the same calculation methods taking into account strong electron correlation as were earlier used by us to study hole cuprates.

Note that strong electron correlation is of fundamental importance and should be correctly taken into account. Indeed, one-electron band calculations give the ground state of LCO and NCO in the form of a metal with a half-filled band, which is at variance with experiment. At the same time, the simplest strong electron correlation models like the Hubbard model are excessively simplified, and the degree of their applicability to describing the band structure of a particular substance is not known a priori. Our experience in studying the electronic structure of high-T_C cuprates taking into account strong electron correlation shows [10–12] that the multiband *p–d* model [13] is the most suitable at excitation energies up to 3 eV inside the valence and conduction bands. This model takes into account two *d* orbitals of copper, $d_{x^2-y^2} \equiv d_x$ and $d_{3z^2-r^2} \equiv d_z$. We used the generalized tight binding method to calculate the band structure of quasi-particles taking into account strong electron correlation [14]. In this method, the many-electron Hamiltonian within the cell is exactly diagonalized, many-electron molecular orbitals are found, and Hubbard *X*-operators are constructed at the first stage. At the second stage, intercell jumps are included and the band structure of the crystal is calculated. Particular examples of calculations of hole cuprates by this method are given in [11, 12, 15].

In this work, we calculated the spectral density and dispersion for the conduction band in compounds undoped and weakly doped with electrons. The calculations by the generalized tight binding method were performed for NCCO with the *T'* structure and *n*-type La_2CuO_4 with the *T* structure. We show that there is a virtual level typical of systems with strong electron correlation both at the bottom of the conduction band and at the top of the valence band [11] in LCO and NCO. The positions of this level in the two compounds are, however, different. The observed asymmetry also results in different concentration dependences of the Fermi level in NCCO and *n*-LCO. The character of valence band dispersion remains virtually identical in compounds of both types. All results obtained for *n*-LCO have no experimental analogs and are predictive in character, because no *n*-LCO materials with the *T* structure have been prepared as yet. In particular, *n*-type superconducting compositions $La_{2-x}Ce_xCuO_4$ obtained in [16] had the *T'* structure. Nevertheless, there is a possibility of inverting *p*-type LCO by the field effect, as with field-effect transistors, where applying a positive voltage to the gate results in the formation of an inversion layer in a *p*-type semiconductor at the boundary with the gate. A theoretical study of the electronic structure of *n*-LCO with the *T* structure is therefore of interest.

In Section 2, we discuss the most important changes in the generalized tight binding method for *n*-type cuprates and give the initial equations for dispersion relations and spectral density. The dispersion dependences for the conduction band in NCCO in comparison with similar dependences for *n*-LCO and experimental dependences are studied in Section 3. In Section 4, we calculate the partial contributions of various orbitals to the spectral density of the conduction band and study the density of states at the bottom of the conduction band in both compounds. The positions of the Fermi level in NCCO at various doping component concentrations are determined in Section 5, where the instability of the state with a uniform charge density distribution is also studied. The results of our calculations are briefly summarized in Section 6.

2. DISPERSION RELATIONS AND SPECTRAL DENSITY OF QUASI-PARTICLE STATES IN NCCO AND *n*-LCO

In the generalized tight binding method, the Hamiltonian of the CuO_2 layer can be written in the form

$$H = \sum_{i\lambda\sigma} \varepsilon_i^{\lambda} a_{i\lambda\sigma}^{\dagger} a_{i\lambda\sigma} + \frac{1}{2} \sum_{i,j} \sum_{\lambda_1\lambda_2\sigma_1\sigma_2\sigma_3\sigma_4} V_{ij}^{\lambda_1\lambda_2} a_{i\lambda_1\sigma_1}^{\dagger} a_{i\lambda_1\sigma_3} \times a_{i\lambda_2\sigma_2}^{\dagger} a_{i\lambda_2\sigma_4} + \sum_{\langle i,j\rangle} \sum_{\lambda_2\lambda_2\sigma} t_{ij}^{\lambda_1\lambda_2} a_{i\lambda_1\sigma}^{\dagger} a_{j\lambda_2\sigma}. \quad (1)$$

Here, $a_{i\lambda\sigma}$ is the hole annihilation operator in the Wannier state on node *i* (copper or oxygen) for orbital λ and spin σ. Two copper orbitals ($d_{x^2-y^2}$ and d_{z^2}) and two $p_{x/y}$ and p_z orbitals on each oxygen node that form σ bonds with the specified copper orbitals are included. Among the Coulomb matrix elements, we can identify intraatomic Hubbard elements $U_d(U_p)$ for repulsion in one copper (oxygen) orbital between electrons with opposite spins, interorbital Coulomb elements $V_d(V_p)$,

$J_d(J_p)$ exchange matrix elements, and interatomic Coulomb repulsion parameters V_{pd}, which we, for simplicity, consider identical for all orbitals. The last term in (1) describes interatomic copper–oxygen jumps with the parameters $t_{pd}^{x^2-y^2,\,x/y} \equiv t_{pd}$ and $t_{pd}^{z^2,\,x} \equiv t_{pd}/\sqrt{3}$ and oxygen–oxygen jumps with the parameter $t_{pp}^{x,\,y} \equiv t_{pp}$. The charge transfer energy will be denoted by $\Delta_{pd} = \varepsilon_p - \varepsilon_{d_{x^2-y^2}}$, and the energy of splitting of the d level in the uniaxial crystal field component, by $\Delta_d = \varepsilon_{dz^2} - \varepsilon_{d_{x^2-y^2}}$. Of six O^{2-} ions, two apical ones are situated along the c axis in the T structure of the LCO composition. Their effects are controlled by two calculation parameters, t'_{pd} and t'_{pp}, which are the integrals of electron jumps from copper and in-pane oxygen to apical oxygen.

In the generalized tight binding method, the band structure of quasi-particles including strong electron correlation effects is calculated in two stages. At the first stage, the CuO_2 layer lattice is partitioned into many unit cells, and the Hamiltonian within one cell is exactly diagonalized. In addition to selecting the CuO_6 cluster as the unit cell, the problem of constructing the Wannier functions of b_{1g} and a_{1g} symmetry on the initial oxygen orbitals is solved [11, 12]. The many-electron molecular orbitals $|n, p\rangle$ (where $n = 0, 1, 2, \ldots$ is the number of holes in the cell and p denotes the set of the other orbital and spin indices) obtained by diagonalizing the cell Hamiltonian H_0 are used to construct the Hubbard operators of this cell, $X^m = |n+1, p\rangle\langle n, q|$, and one-electron operators, $a_{f\lambda\sigma} = \sum_m \gamma_{\lambda\sigma}(m) X^m_{f\sigma}$. Here, the band index of quasi-particles m numbers one-electron excitations from the initial state $|n, q\rangle$ to the final state $|n+1, p\rangle$ [17].

As distinguished from LCO, oxygen and rare-earth metal elements in NCO are known to form their own separate planes in the environment of the CuO_2 plane, and the plane of the rare-earth metal is closest to the CuO_2 plane. In this situation, both parameters should be close to zero, $t'_{pd} = 0$ and $t'_{pp} = 0$. Additional changes in the other parameters were not introduced beforehand and were taken from the calculations of the electronic structure of p-type cuprates [11]. The initial parameters of our Hamiltonian were:

$$\varepsilon_{d_x} = 0, \quad \varepsilon_{d_z} = 2 \text{ eV},$$
$$\varepsilon_p = 1.6 \text{ eV}, \quad \varepsilon_{p_z} = 0.5 \text{ eV},$$
$$t_{pp} = 0.46 \text{ eV}, \quad t'_{pp} = 0, \quad t'_{pd} = 0, \quad U_d = 9 \text{ eV},$$
$$U_p = 4 \text{ eV}, \quad V_{pd} = 1.5 \text{ eV}, \quad J_d = 1 \text{ eV}.$$

In the generalized tight binding method, the dispersion relations and spectral density can be written in the form [11]

$$\left\| \frac{(E - \Omega^G_m)\delta_{mn}}{F^G_\sigma(m)} - 2\sum_{\lambda\lambda'} \gamma^*_{\lambda\sigma}(m) T^{PG}_{\lambda\lambda'}(\mathbf{k}) \gamma_{\lambda'\sigma}(n) \right\| = 0, \quad (2)$$

$$A_\sigma(\mathbf{k}, E) = \left(-\frac{1}{\pi}\right)\sum_\lambda \mathrm{Im}(G^{\lambda\lambda}_{k\sigma}) = \left(-\frac{1}{\pi}\right) \times \sum_{\lambda mn} \gamma_{\lambda\sigma}(m)\gamma^+_{\lambda\sigma}(n)\mathrm{Im}(D^{mn}_{k\sigma}(AA) + D^{mn}_{k\sigma}(BB)), \quad (3)$$

where

$$G^{\lambda\lambda'}_{k\sigma} = \langle\langle a_{k\lambda\sigma} | a^\dagger_{k\lambda'\sigma}\rangle\rangle_E = \sum_{mn} \gamma_{\lambda\sigma}(m)\gamma^\dagger_{\lambda'\sigma}(n) D^{mn}_{k\sigma}, \quad (4)$$

$$\hat{D}_{k\sigma} = \begin{pmatrix} \hat{D}_{k\sigma}(AA) & \hat{D}_{k\sigma}(AB) \\ \hat{D}_{k\sigma}(BA) & \hat{D}_{k\sigma}(BB) \end{pmatrix}, \quad D^{mn}_{k\sigma}(AB) = \langle\langle X^m_{k\sigma} | Y^n_{k\sigma}\rangle\rangle_E. \quad (5)$$

Here, indices P and G run over the A and B antiferromagnetic state sublattices. Equations (2) and (3) were obtained for the antiferromagnetic phase [11, 12] using the equations of motion for Green function (5) in the Hubbard I approximation for intercell jumps. The elements of the tight binding matrix

$$T^{AA}_{\lambda\lambda'}(k) = T^{BB}_{\lambda\lambda'}(k) = \frac{2}{N}\sum_{R_1} T^{AA}_{\lambda\lambda'}(\mathbf{R}_1) e^{ikR_1},$$

$$T^{AB}_{\lambda\lambda'}(k) = T^{BA}_{\lambda\lambda'}(k) = \frac{2}{N}\sum_{R_2} T^{AB}_{\lambda\lambda'}(\mathbf{R}_2) e^{ikR_2}$$

in the five-orbital d_x, d_z, b, a, p_z basis take the form

$$T_{\lambda\lambda'}(\mathbf{R}) = \begin{pmatrix} 0 & 0 & -2t_{pd}\mu_{ij} & 0 & 0 \\ 0 & 0 & \frac{2t_{pd}\xi_{ij}}{\sqrt{3}} & \frac{2t_{pd}\lambda_{ij}}{\sqrt{3}} & 0 \\ -2t_{pd}\mu_{ij} & \frac{2t_{pd}\xi_{ij}}{\sqrt{3}} & -2t_{pp}\nu_{ij} & 2t_{pp}\chi_{ij} & -2t'_{pp}\xi_{ij} \\ 0 & \frac{2t_{pd}\lambda_{ij}}{\sqrt{3}} & 2t_{pp}\chi_{ij} & 2t_{pp}\nu_{ij} & -2t'_{pp}\lambda_{ij} \\ 0 & 0 & -2t'_{pp}\xi_{ij} & -2t'_{pp}\lambda_{ij} & 0 \end{pmatrix}; \quad (6)$$

the μ_{ij}, ξ_{ij}, λ_{ij}, ν_{ij}, and χ_{ij} coefficients were given

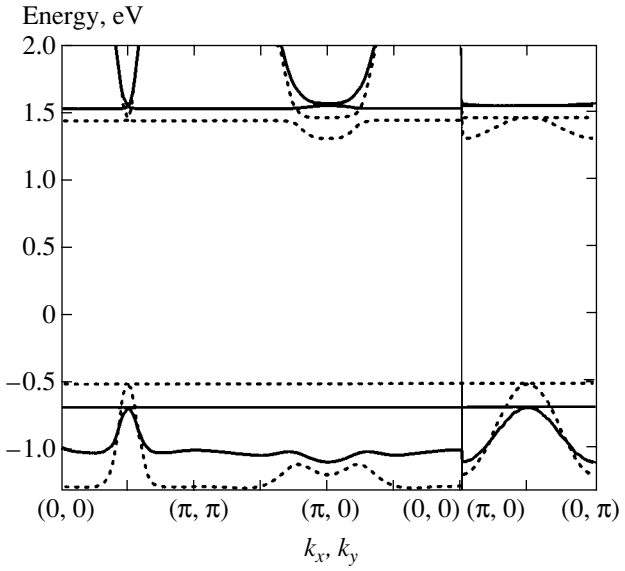

Fig. 2. Dispersion dependences for *n*-LCO (solid line) and NCCO (dotted line). Doping level $x = 0.03$.

in [11]. Equation (2) is an analog of the dispersion equation in the tight binding method and differs from it in two respects. First, quasi-particle energies are calculated in the form $\Omega_m^G = \varepsilon_{2qG} - \varepsilon_{1pG}$, that is, in the form of resonances between many-particle states from different configuration space sectors. Secondly, the occupation number $F_\sigma^G(m) = \langle X_{f_G\sigma}^{pp} \rangle + \langle X_{f_G\sigma}^{qq} \rangle$ leads to concentration dependences of both dispersion and spectral density amplitude (3). Quasi-particle states with different m can overlap and interact, like singlet and triplet two-hole states of *p*-type cuprates do [11, 12].

3. DISPERSION OF BANDS

The band dispersion for *n*-LCO and NCCO at a concentration of the doping *n*-component of $x = 0.03$ in the antiferromagnetic phase is shown in Fig. 2. Calculations only reproduce dispersion in the immediate vicinity of the dielectric gap. This is sufficient for analyzing the spectrum of quasi-particles involved in the superconducting state.

The bottom of the conduction band is formed as a result of the dispersion of the local state with an energy of $\Omega_c = E(1, {}^2b_{1g}) - E(0, a_{1g})$, and the top of the valence band is formed by excitations with the participation of the two-hole singlet $\Omega_v = E(2, {}^1A_{1g}) - E(1, {}^2b_{1g})$ and triplet $\Omega_v^1 = E(2, {}^3B_{1g}) - E(1, {}^2b_{1g})$ (Fig. 3). Both compounds have a virtual level at the bottom of the conduction band. This level is similar in nature to that at the top of the valence band (Fig. 3) [11]. Namely, there are two types of quasi-particles that correspond to possible transitions Ω_c and Ω_v. One of the quasi-particles in the undoped compound corresponds to the transition between empty states, which gives zero contributions to dispersion and spectral density. In the one-hole sector of the configuration space, the empty state is one of the components of the spin doublet in each of the sublattices of the Néel antiferromagnetic state of the CuO_2 layer. The vacuum sector corresponds to the a_{1g} singlet state of the fully occupied p^6d^{10} shell. The existence of two singlet states in the vacuum and two-hole sectors (Fig. 3) is the main reason for the existence of the dispersionless virtual level not only at the top of the valence band but also at the bottom of the conduction band in *n*-LCO and NCCO.

Conduction band dispersion in *n*-LCO was calculated with the parameter values obtained in studying the

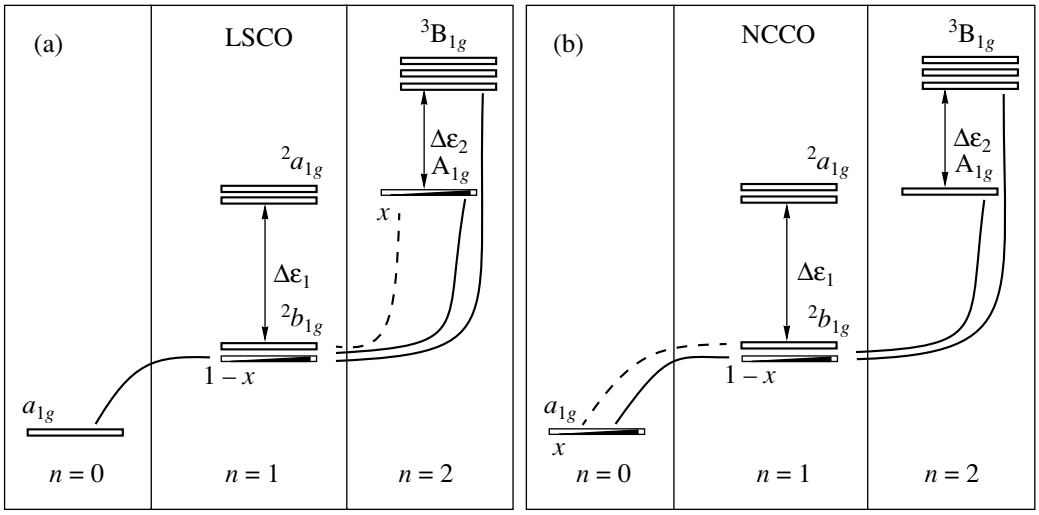

Fig. 3. Configuration space scheme for LSCO and NCCO. The solid lines correspond to quasi-particle transitions that form rigid bands, and the dashed lines, to impurity bands.

electronic structure of *p*-type cuprates. Mere comparison of the spectra for *n*-LCO and NCCO in Fig. 2 shows that the degeneracy of the spectrum of LCO at point $X = (\pi, 0)$ is accidental. Conversely, the intersection of two conduction bands, the broad band and the band of virtual level states, at point $M = (\pi/2, \pi/2)$ is caused by CuO_2 layer symmetry and does not depend on the parameter values used in the calculations.

The broad band and the band of virtual level states behave differently as the doping level increases [11, 15]. The broad bands remain virtually unchanged; they will further be called rigid by analogy with the rigid band model. The spectral density and dispersion for the virtual level state bands increase as the degree of doping grows, and they will be called "impurity" bands. Quotation marks (further omitted) are not meaningless, because these states have no bearing on the true local impurity potential.

The transport of quasi-particles in the valence and conduction bands occurs with different effective transport integrals. We therefore observe different dispersion dependences for different bands. Indeed, calculations give $t'_{\text{c.b.}}/t_{\text{c.b.}} = -0.05$ and $t'_{\text{v.b.}}/t_{\text{v.b.}} = -0.14$ for NCO and $t'_{\text{c.b.}}/t_{\text{c.b.}} = 0.05$ and $t'_{\text{v.b.}}/t_{\text{v.b.}} = -0.085$ for LCO, where $t_{\text{c.b.}}$ ($t'_{\text{c.b.}}$) and $t_{\text{v.b.}}$ ($t'_{\text{v.b.}}$) are the effective transport integrals between the nearest (next-nearest) neighbors for the conduction and valence bands, respectively. The most significant change in passing from LCO to NCO is the formation of a nonlinear dielectric gap because of the formation of a new minimum at the *X* point of the conduction band. Calculations show that the appearance of a rectilinear gap is also accompanied by a change in the sign of the $t'_{\text{c.b.}}/t_{\text{c.b.}}$ ratio. There are moderate changes in the valence band, but they do not lead to qualitative differences in the dispersion dependences for the *n* and *p* materials.

The reproduction of dispersion at the bottom of the conduction band in NCCO requires the initial parameters to be changed as follows:

$$\varepsilon_{d_x} = 0.2 \text{ eV}, \quad \varepsilon_{d_z} = 2 \text{ eV},$$
$$\varepsilon_p = 1.6 \text{ eV}, \quad \varepsilon_{p_z} = 0.5 \text{ eV},$$
$$t_{pp} = 0.56 \text{ eV}, \quad t'_{pp} = 0.1 \text{ eV},$$
$$t'_{pd} = 0, \quad U_d = 9 \text{ eV},$$
$$U_p = 4 \text{ eV}, \quad V_{pd} = 1.5 \text{ eV}, \quad J_d = 1 \text{ eV}.$$

It follows that dispersion calculations in NCCO largely result in changes in the t'_{pd} and t'_{pp} values and, to a lesser extent, in Δ_{pd} and t_{pp}. A smaller Δ_{pd} value corresponds to a smaller dielectric gap in NCO, $E_g = 1.6$ eV. A smaller t_{pp} value in LCO in turn corresponds to the presence of orthorhombic distortions in the system of CuO_6 octahedra. As a consequence, a small increase in t_{pp} in NCCO is responsible for the conduction band minimum at point *X* at low electron concentrations. In combination, changes in precisely these parameters qualitatively modify the dielectric gap and make it nonlinear in NCO.

Among the known materials based on *n*-LCO and having the *T* structure, the calculated dispersion might be observed in $La_2Cu_{1-x}Zn_xO_4$ compositions [1], because Zn^{2+} has a completely filled d^{10} shell, which formally corresponds to filling the vacuum sector, as in *n*-type materials such as NCCO. However in reality, the Zn impurity leads to a strongly bound carrier and the violation of translational invariance over the spin lattice. It appears that, because of strong impurity effects, photoemission measurements for $La_2Cu_{1-x}Zn_xO_4$, similar to those performed for NCCO [5], cannot be made.

4. PARTIAL CONTRIBUTIONS TO SPECTRAL DENSITY

We calculated the spectral density $A(\mathbf{k}, E)$ for the rigid and impurity bands in NCCO (Fig. 4) at a low concentration of the doping component $x = 0.03$. The spectral density is characterized by two peaks corresponding to the rigid and impurity bands. The dependences of the peak amplitudes for (a) the rigid and (b) impurity bands along the symmetrical Brillouin zone directions are plotted in Fig. 4. Figure 5b shows how the virtual level with zero spectral weight at $x = 0$ transforms into an impurity band with spectral weight *x*. The overshooting of triplet states into the conduction band is insignificant, and this is one more source of asymmetry of the states of *p*- and *n*-type carriers. Similar dependences for the conduction band in *n*-LCO are shown in Fig. 5. These results cannot however be compared with experimental data because of the absence of *n*-type compounds based on LCO with the *T* structure.

As follows from calculations of the density of states, there is a region with a reduced density between the impurity and rigid bands (Fig. 6). This pseudogap vanishes at point $\overline{M} = (\pi/2, \pi/2)$ (Fig. 2). For this reason, the passage of the Fermi level from the rigid to the impurity band may be accompanied by a decrease in the density of states on this level. The pseudogap itself is magnetic in nature, as follows from its absence in the paramagnetic phase. Because of the special features inherent in the spectrum, the pseudogap is more pronounced for the density of states of NCCO.

5. THE CONCENTRATION DEPENDENCE OF THE FERMI LEVEL

Calculations of the dependence of the Fermi level position on doping in NCCO for the antiferromagnetic phase exhibit considerable differences from the dependence obtained for *n*-LCO. Indeed, at low concentrations, the Fermi level in NCCO goes deep into rigid

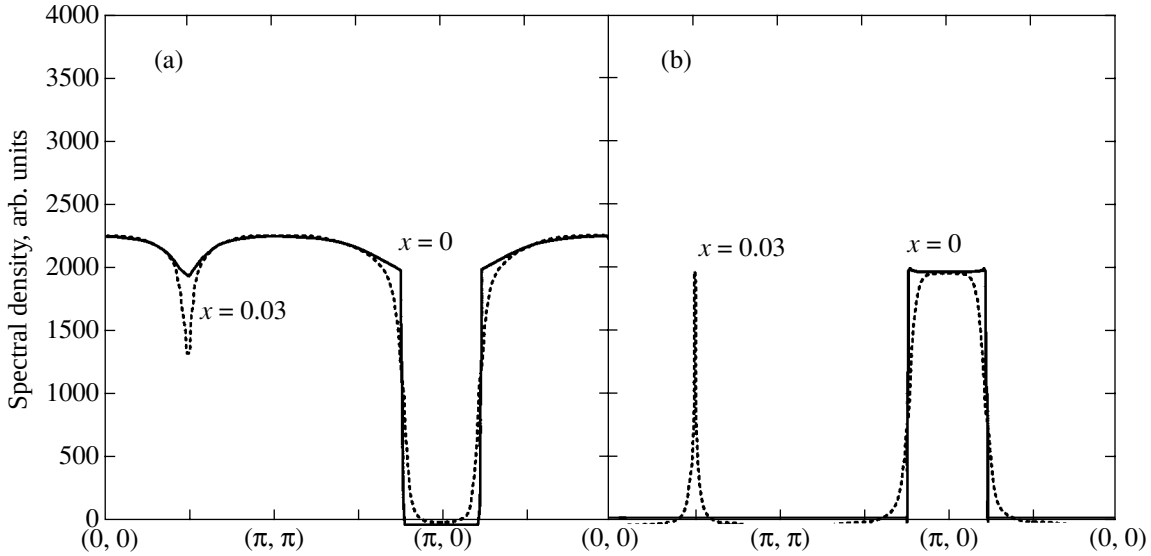

Fig. 4. Spectral density of quasi-particle states along symmetrical Brillouin zone directions in NCO (a) for the rigid conduction band and (b) for the band of virtual level states.

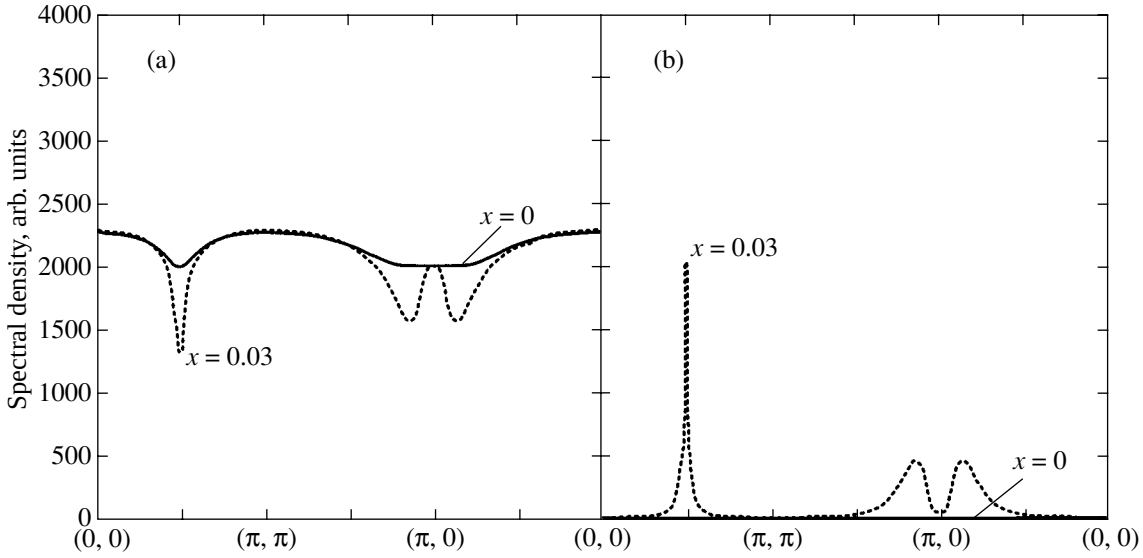

Fig. 5. Spectral density of quasi-particle states along symmetrical Brillouin zone directions in *n*-LCO (a) for the rigid conduction band and (b) for the impurity band.

conduction band states and only then, at $x = x_1$, into impurity band states. This corresponds to $x_1 = 0.08$–0.1 in Fig. 7. The Fermi level reenters rigid band states at $x_2 = 0.18$–0.2. A similar dependence of the Fermi level in *n*-LCO shows pinning only at low concentrations. Indeed, already at very low concentrations, the Fermi level occurs in the zone of impurity band states that are being formed. Because the number of states on the Fermi level begins to grow more slowly than x (Fig. 8b), pinning ends, and the Fermi level enters the rigid conduction band. This occurs at $x_2 = 0.11$–0.12.

The calculated concentration dependence of the Fermi level contains a Δx interval where the rate of growth of the number of states in the impurity band exceeds the rate of increasing the number of carriers $\partial\mu/\partial x = (\partial^2\Phi/\partial x^2)_{T,P} < 0$, which is evidence of possible phase stratification at the given doping level. Such compositions cannot be stably homogeneous, because the sought distribution corresponds to the thermodynamic potential Φ maximum. For instance, the dependence of $\partial\mu/\partial x$ on x for NCCO (Fig. 9) shows that $\Phi(x)$ has an instability region $\Delta x \approx 0.03$ wide. This region separates

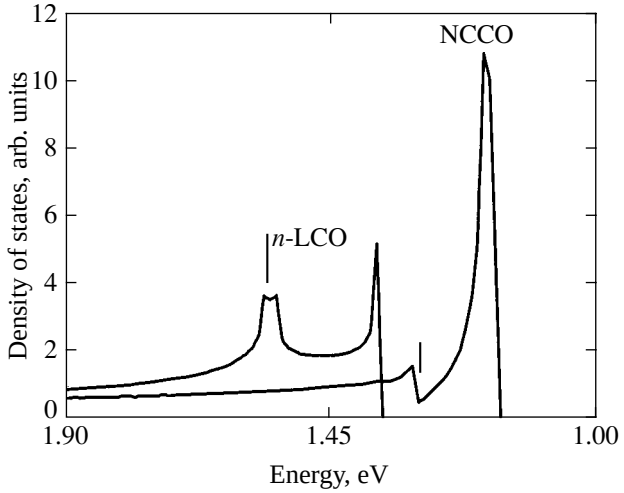

Fig. 6. Density of states at the bottom of the conduction band in NCCO and *n*-LCO. The vertical line indicates the region with a reduced density of states (pseudogap).

two regions with thermodynamic potential minima. Even at small dopant concentrations, *n*-LCO occurs in the $\Delta x \approx 0.05$ region with a maximum thermodynamic potential. Although the materials under consideration are systems with fixed numbers of carriers, both systems can either be divided into macroscopic regions capable of exchanging particles or experience the transition to the superconducting state, where the number of particles is no longer conserved. The origin of the instability of the homogeneous normal state is related to the presence of antiferromagnetic order, because the impurity band disappears in the paramagnetic phase. It follows that we observe an unusual relation between the nonuniform charge density distribution and the presence of antiferromagnetic ordering. The inclusion of zero spin fluctuations causes instability region Δx narrowing, but does not negate its existence [15].

We also observe a qualitative correlation between Fermi level movement to the antiferromagnetic state and the phase diagram of NCCO. Indeed, the concentration region of Fermi level residence in the impurity band, or, which is the same, in the pseudogap region correlates with the superconducting region in the phase diagram. In NCCO and *n*-LCO, the Fermi level reaches the pseudogap at different dopant concentrations $x_1(\text{NCCO}) > x_1(n\text{-LO}) = 0$. In NCCO, the Fermi level enters impurity band states with an already well-developed spectral density. This is seen from Fig. 8a, where the spectral density in the impurity band is nonzero already at $x = x_1$. It follows that the presence of a finite spectral density of impurity band states at the Fermi level corresponds to the superconducting region in the phase diagram of NCCO. The immediate consequence of a correlation of this type would be the beginning of the superconducting region in the phase diagram of NCCO at T_C higher than T_C for *n*-LCO, this region being narrower on the concentration scale. Accordingly, we also have $x_{max} \approx x_2$. Such an equality was observed for PCCO in [18], whose authors were able to

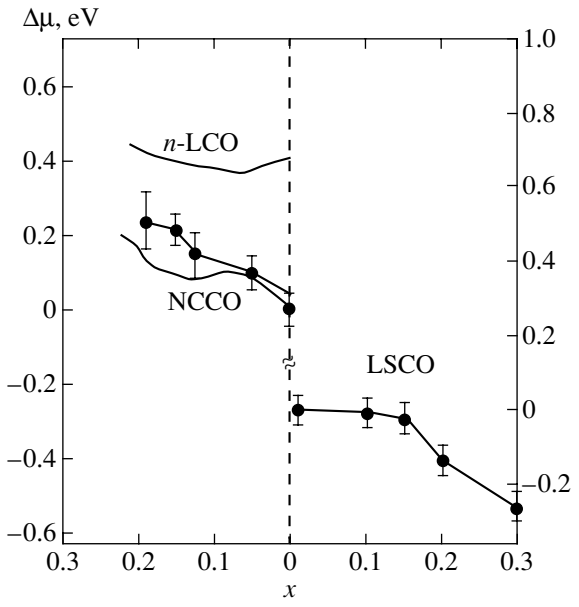

Fig. 7. Dependence of the chemical potential shift $\Delta\mu(x)$ on the concentration of the doping *n*-component in NCCO and *n*-LCO. The experimental data on NCCO and LSCO were taken from [6].

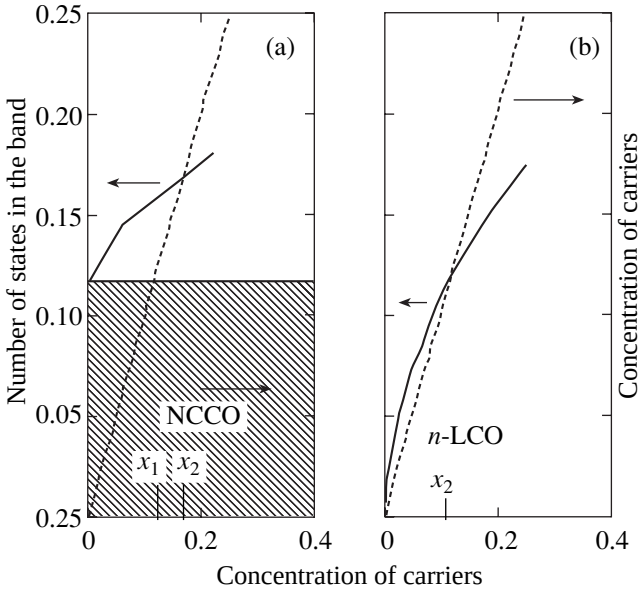

Fig. 8. Dependence of the total number of states on the concentration of the doping component for the impurity bands in NCCO and *n*-LCO; x_1 and x_2 correspond to the entrance to and exit from the band of virtual level states, respectively. The solid line shows the number of states, and the dashed line, the concentration of electrons *x*. The shaded region in (a) corresponds to the contribution of the rigid band.

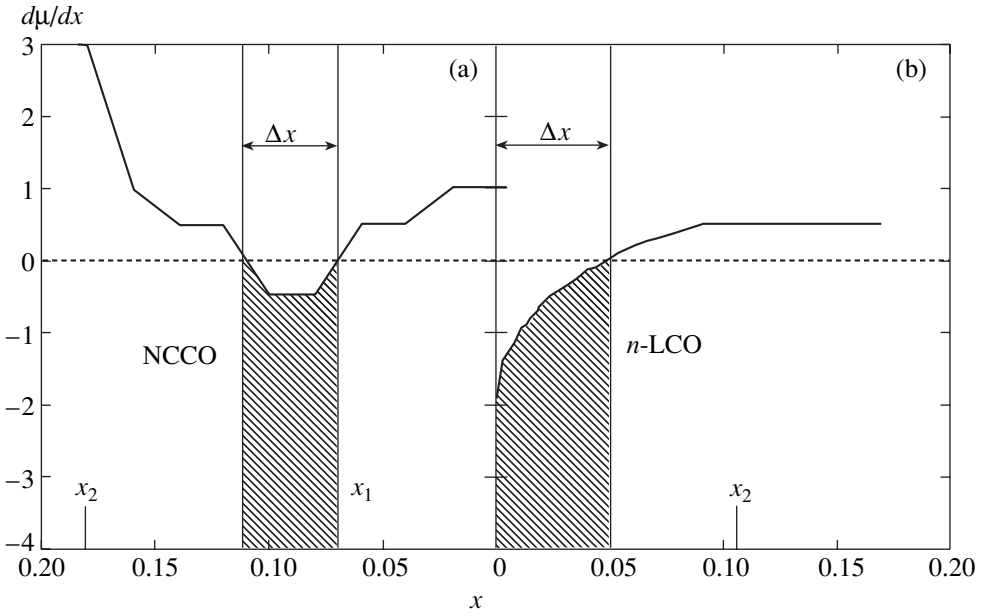

Fig. 9. Dependence of the second thermodynamic potential derivative $\partial^2\Phi/\partial x^2$ on the concentration of the doping component in NCCO and *n*-LCO; x_2 corresponds to the exit of the Fermi level from the impurity band.

study the $T^*(x)$ dependence of the characteristic temperature for the pseudogap state in the superconducting phase of PCCO in magnetic fields higher than H_{c2}. In our calculations, the pseudogap state is an attribute of the impurity band rather than the precursor of the superconducting state. It can be identified as a special feature of the electronic structure of materials with strong electron correlation in the antiferromagnetic phase and with a singlet ground state in one of the configuration space sectors of the unit cell of the material under study.

6. CONCLUSIONS

The results of our calculations can be summarized as follows:

(1) Common to the dispersion dependences for NCCO and *n*-LCO is the presence of a virtual level at the bottom of the conduction band and at the top of the valence band in the antiferromagnetic phase. The reason for its existence is the presence of singlet states in the vacuum (a_{1g} is a closed shell) and two-particle (A_{1g}) configuration space sectors of both compounds. The rigid conduction band in NCCO has a minimum at point *X* of the Brillouin zone at low doping levels. Because of accidental degeneracy of the rigid band and virtual level at point *X* in *n*-LCO, its dielectric gap is rectilinear, whereas the gap in NCCO is not. The last conclusion is in agreement with the angle-resolved photoelectron spectroscopy data on weakly doped NCCO compounds [5].

(2) The concentration dependences of the Fermi level for NCCO with the *T*' structure and *n*-type LCO with the *T* structure are not symmetrical. We explain this asymmetry by the different positions of the virtual level with respect to the bottom of the rigid conduction band in these compositions. As a consequence, we observe pinning of the Fermi level by states developed on the virtual level in *n*-type LCO at low dopant concentrations. In NCCO, the Fermi level is immediately immersed into rigid conduction band states and only enters impurity band states when the degree of doping increases further. The probability of pinning the Fermi level by them, however, actually decreases as the doping level grows.

(3) We observed that, in our calculations, the regions of Fermi level pinning by the impurity band were virtually Δx regions with an instability of the form $(\partial^2\Phi/\partial x^2)_{T,P} < 0$, which could be the reason for a nonuniform charge density distribution in the compositions under consideration.

(4) A qualitative correspondence exists between the phase diagram of NCCO and the concentration dependence of the Fermi level: namely, the concentration region of Fermi level residence in the impurity band correlates with the concentration region of the superconducting state in these compounds. There is no such correspondence for *n*-LCO because of the absence of the corresponding materials with the *T* structure. Our results, however, show that the hypothetical phase diagram for LCO of the *p*/*n* type with the *T* structure should be more symmetrical than the diagram of NCCO/LSCO.

ACKNOWLEDGMENTS

This work was financially supported by the Russian Foundation for Basic Research (project no. 03-02-16124), RFFI-KKFN "Eniseĭ" (project no. 02-02-97705),

INTAS (project no. 01-0654), integration program of URO and Siberian Division, Russian Academy of Sciences (project no. 9), and the "Quantum Macrophysics" program of the Russian Academy of Sciences.

REFERENCES

1. B. Keimer, N. Belk, R. J. Birgeneau, *et al.*, Phys. Rev. B **46**, 14034 (1992).
2. S. G. Ovchinnikov, Physica C (Amsterdam) **228**, 81 (1994).
3. S. J. Hagen, J. I. Peng, Z. Y. Li, and R. I. Greene, Phys. Rev. B **43**, 13606 (1991).
4. H. Takagi, B. Batlog, H. L. Kao, *et al.*, Phys. Rev. Lett. **69**, 2975 (1992).
5. N. P. Armitage, F. Ronning, D. H. Lu, *et al.*, Phys. Rev. Lett. **88**, 257001 (2002).
6. N. Harima, J. Matsuno, A. Fujimori, *et al.*, Phys. Rev. B **64**, 220507(R) (2001).
7. P. Fulde, Physica B (Amsterdam) **230**–**232**, 1 (1997).
8. W. Henggeler, B. Roessli, A. Furrer, *et al.*, Phys. Rev. Lett. **80**, 1300 (1998).
9. E. Maiser, W. Mexner, R. Schafer, *et al.*, Phys. Rev. B **56**, 12961 (1997).
10. S. G. Ovchinnikov, Usp. Fiz. Nauk **167**, 1043 (1997) [Phys. Usp. **40**, 993 (1997)].
11. V. A. Gavrichkov, S. G. Ovchinnikov, A. A. Borisov, and E. G. Goryachev, Zh. Éksp. Teor. Fiz. **118**, 422 (2000) [JETP **91**, 369 (2000)].
12. V. A. Gavrichkov, A. A. Borisov, and S. G. Ovchinnikov, Phys. Rev. B **64**, 235124 (2001).
13. Ya. B. Gaididei and V. M. Loktev, Phys. Status Solidi B **147**, 307 (1988).
14. S. G. Ovchinnikov and I. S. Sandalov, Physica C (Amsterdam) **161**, 607 (1989).
15. A. A. Borisov, V. A. Gavrichkov, and S. G. Ovchinnikov, Zh. Éksp. Teor. Fiz. **124**, 862 (2003) [JETP **97**, 773 (2003)].
16. M. Naito and M. Hepp, Jpn. J. Appl. Phys. **39**, L485 (2000).
17. R. O. Zaĭtsev, Zh. Éksp. Teor. Fiz. **68**, 207 (1975) [JETP **41**, 100 (1975)].
18. L. Alff, Y. Krockenberger, B. Welter, *et al.*, Nature **422**, 698 (2003).

Translated by V. Sipachev